Design of a Low-Voltage, Axially Modulated, Cusp-Injected, Third Harmonic, X-Band Gyrotron Amplifier Experiment

Arnold Liu, Wes Lawson, *Senior Member, IEEE,* Anna Fernandez, *Member, IEEE,* John Rodgers, and William W. Destler, *Fellow, IEEE*

***Abstract*— We present the design of a prebunched, third harmonic small-orbit gyrotron experiment that utilizes a 45 kV, 8 A beam to produce over 185 kW of amplified power at 9.9 GHz in a 1.23 kG magnetic field. We detail the design of the electron gun, which produces a moderately compressed axially streaming annular beam. The beam is velocity modulated by a short TM_{010} coaxial input cavity and energy is extracted in a right-circular TE_{021} output cavity. Perpendicular energy is imparted to the beam via a nonadiabatic magnetic transition at the end of a 23 cm drift region between the two cavities. A nonlinear single particle code is used to predict an electronic efficiency of 52% and a large signal gain of 25.5 dB. This code generates the cavity field profiles via a scattering matrix formalism and uses the output from the electron gun code to model the beam. This improved model allows the potentially important effects of leakage fields and finite beam thickness and spread to be investigated.**

I. Introduction

CONVENTIONAL gyrotron oscillators and amplifiers operating near the first harmonic of the cyclotron frequency have been proven to be reliable, efficient, high power sources of microwave and millimeter wave radiation [1]–[3]. These sources have potential applications as RF drivers for accelerators, plasma heating and current drives in magnetic fusion research, and millimeter wave and deep space radars, as well as applications in materials processing and nonlinear spectroscopy of semiconductors and biological materials.

Unfortunately, gyrotrons operating near the cyclotron frequency must be immersed in a magnetic field whose strength is proportional to the output frequency. Consequently, they are not viable candidates for some high-frequency applications that require compact and lightweight tubes. Two potential ways to decrease the required magnetic field are 1) to use Doppler upshifting via operation at a high axial wavenumber, and 2) to operate at an harmonic of the cyclotron frequency. The cyclotron auto-resonance maser (CARM) is an example of a device that takes the first approach [4], [5]. Several CARM's have been built and tested but none have come close to the best efficiencies achieved in conventional gyrotrons. Mode competition from gyrotron instabilities and sensitivity to velocity spread have been the principle limiting factors. Low harmonic operation (typically the second or third harmonic) has met with some success in the conventional small-orbit gyrotron configuration [6]–[8], and high-harmonic devices have been quite successful in the large-orbit configuration [9]–[20]. Nonetheless, the best efficiencies in second harmonic devices are usually a few percent less than their first harmonic counterparts and beyond the second harmonic efficiencies tend to decrease rapidly with increasing harmonic number.

We have proposed [21] a method of electron beam prebunching in high harmonic, large-orbit devices based on the cusp-injection scheme, which can significantly enhance efficiency [22]. In this scheme, an annular beam encounters a circularly polarized TM_{mn0} mode input cavity and a subsequent drift region before it passes through the balanced, nonadiabatic magnetic field reversal. If done properly, the resultant ballistic bunching sets up a beam that can efficiently interact at the mth harmonic with a simple right-circular output cavity. In a recent effort, we demonstrated that this prebunching scheme could be extended to a second harmonic small-orbit system via a non-adiabatic transition, which does not reverse the direction of the magnetic field [23].

In this paper, we present the design of a small-orbit system that we expect to fabricate and test at the University of Maryland. In this design, a 45 kV, 8 A annular beam is prebunched by a TM_{010} coaxial cavity and interacts at the third harmonic of the cyclotron frequency with a TE_{021} cavity to theoretically produce over 185 kW of power with an efficiency and large-signal gain of approximately 52% and 25.5 dB, respectively. In Section II, we discuss the electron gun geometry and present the simulated performance characteristics. In Section III, we present the design of the microwave circuit, detail the tube stability and large-signal properties, and characterize the sensitivity of the device to parameter variations. We also describe the models and computer codes used in the analysis. Three notable improvements in our modeling techniques (as compared to previously reported designs [21], [23]) include the use of beam parameters generated by an electron gun code, the incorporation in some regions of magnetic field profiles from actual coils, and the use of a scattering matrix code to generate the field profiles in both cavities. The results of this study are summarized in the final section.

II. Electron Gun Design

The nominal beam parameters for the third harmonic system are given in Table I. The beam voltage and current are limited

Manuscript received July 30, 1996; revised April 22, 1997. This work was supported by the Tri-Services Program for Vacuum Electronics. The review of this paper was arranged by Editor James A. Dayton, Jr.

The authors are with the Electrical Engineering Department and Institute for Plasma Research, University of Maryland, College Park, MD 20742 USA (e-mail: lawson@eng.umd.edu).

Publisher Item Identifier S 0018-9383(97)07741-1.

TABLE I
THIRD HARMONIC SMALL-ORBIT AMPLIFIER SYSTEM DESIGN PARAMETERS

Beam Voltage (kV)	45	
Beam Current (A)	8	
Output frequency (GHz)	9.9	
	(before cusp)	(after cusp)
Average radius (cm)	2.30	1.74
Beam thickness (cm)	0.15	1.27
Velocity ratio ($v_\perp/v_z$)	0.00	2.20
Magnetic field (kG)	0.632	1.234

TABLE II
ELECTRON GUN SPECIFICATIONS AND SIMULATED PERFORMANCE

Emitter radius (cm)	3.8
Emitter width (cm)	0.2
Emitter angle (deg)	-11.5
Cathode loading (A/cm^2)	1.68
Cathode magnetic field (G)	221
Cathode-Anode gap (cm)	3.0
Average velocity ratio	0.02
Axial velocity spread (%)	0.02
Average beam radius (cm)	2.24
Beam thickness (cm)	0.033
Peak anode field (kV/cm)	30.2
Peak cathode field (kV/cm)	36.3
Average emitter field (kV/cm)	9.5
Space-charge current limit (A)	11.5

in part by the availability of a modulator and by the desire to construct a compact device. The output frequency for this proof-of-principle experiment is selected in accordance with available microwave sources and magnetic field coils and supplies. The magnetic field in the output cavity is set to a value that nominally yields a cyclotron frequency that is one-third the value of the drive frequency. The beam radius after the magnetic cusp is set to maximize the efficiency of the interaction and the precusp radius and precusp magnetic field are determined by canonical angular momentum given the parameters mentioned previously and the average ratio of the electrons' perpendicular velocity to parallel velocity. This ratio is selected as a trade-off between the desire for more perpendicular energy and the need to keep the axial velocity spread within reasonable limits.

A schematic of the overall system is shown in Fig. 1. The magnetic field on the upstream (cathode) side of the iron pole piece is generated by four pancake coils. The flat field region has a maximum ripple of $\pm 1.0\%$. The magnetic field on the output cavity side is generated by three coils. The iron plate has a diameter of 17.8 cm and a maximum thickness of 1.8 cm. Near the beam radius, the iron thickness is reduced to 0.5 cm to minimize the transition length of the nonadiabatic region. The inner conductor is supported at the iron plate and near the input cavity.

The electrode configuration of the electron gun is also plotted in Fig. 1 along with the axial field profile on axis and the simulated ray trajectories for the beam. The electrode specifications are given in Table II. The ratio of the emitter width to the average radius should result in an ideal perpendicular velocity spread of about 1.5% (and an axial velocity spread of 7.4%) from canonical angular momentum considerations. The cathode field is determined by the required beam compression and the cathode angle is adjusted so that the beam will initially follow the magnetic field lines. The average current density at the cathode is quite reasonable even for continuous (CW) operation. The length of the magnetic compression region, which we define to be the distance between the emitter strip and the entrance to the input cavity, is 17 cm.

The electron gun operation was simulated with the EGUN trajectory code [24] and the results are indicated in the lower half of Table II. All beam parameters are given at the center of the input cavity and are close to their design goals. The beam is almost completely axial in nature, with the perpendicular motion accounting for less than 0.04% of the total energy. The peak electric field in the gun occurs at the tip of the cathode

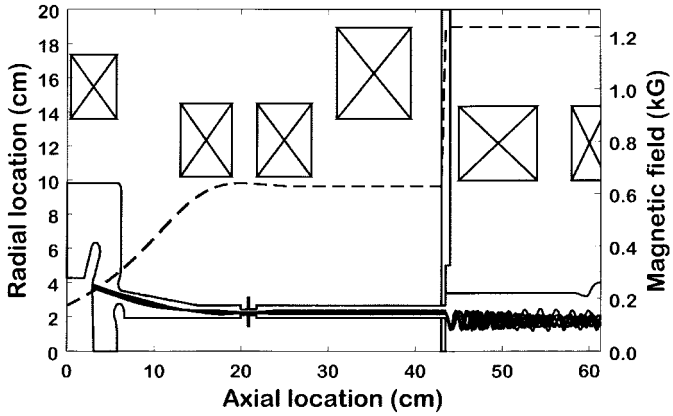

Fig. 1. Schematic of the third harmonic system and the simulated beam trajectory. The axial magnetic field profile on axis is indicated by the dashed line.

focus electrode and is also suitable for CW operation. The peak field on the anode occurs near the entrance to the beam tunnel and is 20% less than the peak cathode field. The space charge limiting current is 44% above the operating current, indicating that the gun will be run temperature limited and that higher output powers may be possible.

III. MICROWAVE CIRCUIT DESIGN

Given the magnetic field profile and beam trajectory results of the EGUN simulation, four additional codes are utilized to design the microwave circuit. First, a scattering matrix [25] code is used to design the input and output cavities. This code calculates the resonant frequency of each cavity, the diffractive quality factor (Q_D), the resistive Q_R, and the electromagnetic (EM) field profiles. The use of this code is necessary to accurately account for the leakage fields in the drift region (which is particularly important near the input cavity) and in the output waveguide.

Next, a linear start-oscillation code [26] is used to check the stability of the cavities to spurious modes. This code assumes that the magnetic field is constant in each cavity and uses the field profiles from the scattering matrix code. The output

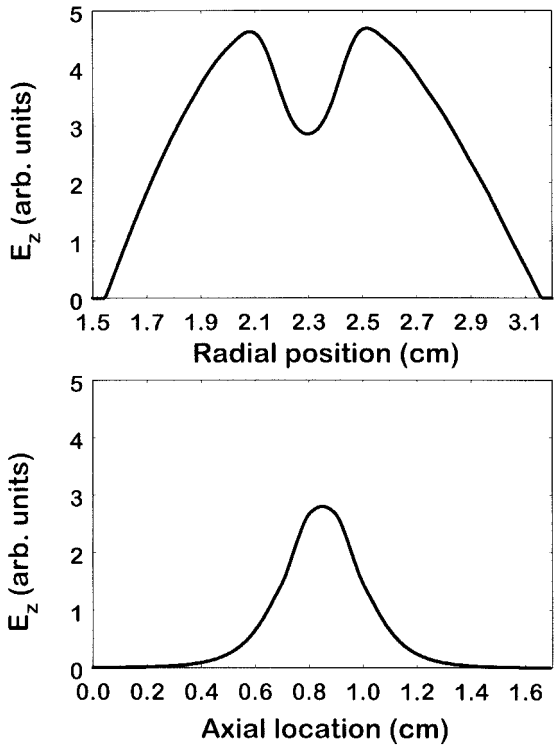

Fig. 2. Axial electric field in the input cavity (a) as a function of radial location and (b) as a function of axial position.

cavity stability is checked for an unbunched beam and the input cavity stability is often taken for granted, since the cavity is short and the beam streams linearly through it.

The other two codes are single particle large-signal codes that numerically integrate the particle motion in the device. Both use the same numerical integration scheme, which is a fourth order Milne predictor followed by a fourth order Adams–Moulton corrector (with a Runga–Kutta start-up). The differences in the codes stem from the assumed tube geometry and the input and output information. Numerical convergence is checked by varying integration step size and the number of particles. Conservation of energy and canonical angular momentum are also checked in regions where there is only a static magnetic field.

The first large-signal code simulates the beam's motion through the input cavity, the drift region, and the nonadiabatic magnetic transition. This "bunching" code can use a different time step in each of those regions. EGUN supplies the beam distribution in radius and velocity. The code then "launches" those rays over a range of initial times and angles that represent the entirety of phase space (after taking into account any symmetries in the system). Given the coil geometry, the magnetic field in the drift region is computed from the vector potential. However, the magnetic field in the transition region is approximated with a piecewise linear axial field profile. This code produces the phase space distributions of the electrons at the end of the transition region and calculates various quantities that give the average beam statistics and indicate the effectiveness of the bunching process. The required drive power for the assumed electric field strength is also reported. This code is typically iterated, while adjusting the drift region length and the electric field magnitude, until satisfactory bunching performance is achieved.

The second large-signal code takes the output from the first single particle code and the scattering matrix results for the output cavity and calculates the extraction efficiency of the EM wave in the output cavity under steady-state conditions. For simplicity, the magnetic field in the output cavity is assumed to vary linearly. This "efficiency" code is typically iterated, while varying the cavity and magnetic field parameters, until an optimal design is achieved. During each efficiency run, the amplitude and phase of the EM wave are adjusted until maximum efficiency is calculated. In addition to the efficiency, the code reports the required total Q. The cavity design must be iterated until the Q's from the efficiency code and the scattering matrix code are consistent. By decreasing the field amplitude in the output cavity toward zero, this code can also be used to calculate the start currents for the various modes in tapered magnetic fields, whether or not the beam is prebunched.

The length and the inner and outer radii of the main section of the input cavity are 0.20, 1.55, and 3.16 cm, respectively. The resonant frequency of the cavity is 9.9 GHz in the TM_{010} coaxial operating mode. The diffractive Q is 36 340 and the resistive Q is 2380. The diffractive Q comes predominantly from the energy leakage that results from coupling to the TEM mode at the end of the main input cavity section. The length of cutoff sections on either side of the main cavity are selected to minimize this leakage, and are approximately a quarter wavelength long. The gap between inner and outer radii leaves approximately 1 mm clearance for the beam. The inner and outer radii of the beam tunnels adjacent to the cavity are 1.9 and 2.7 cm, respectively, and are also important in reducing the leakage power. Because Q_D is significantly larger than Q_R, the leakage power should not interfere significantly with the bunching process. Furthermore, the experimental design will have support pins, which will tend to short out the TEM mode. Still, the region adjacent to the cavity will undoubtedly be lined (or coated) with lossy material. In the experiment, the cavity will be excited by a single slot along the outer wall. For critical coupling, the external Q of this slot will be comparable to the cavity Q, so that the total input quality factor should be approximately $Q_T = 1120$. All gain estimates reported in this paper are based on this lower Q value. The axial electric field profile in the input cavity is indicated in Fig. 2. The dependence of E_z at the midpoint of the cavity is given in Fig. 2(a) as a function of radial position. The double maxima are a direct consequence of the opening in the axial walls necessary for beam transmission. The dependence of E_z at the average beam location is plotted in Fig. 2(b) as a function of axial position. The exponential tail of the field in the outer regions is clearly seen.

The evolution of electron bunching in the tube is illustrated in Fig. 3, where the distribution of representative particles relative to the phase of the output cavity's electric field is plotted at various axial locations. Fig. 3(a) shows the distribution at the output cavity entrance when zero drive power is applied and illustrates the initially uniform distribution of particles in phase space. The seven levels of perpendicular

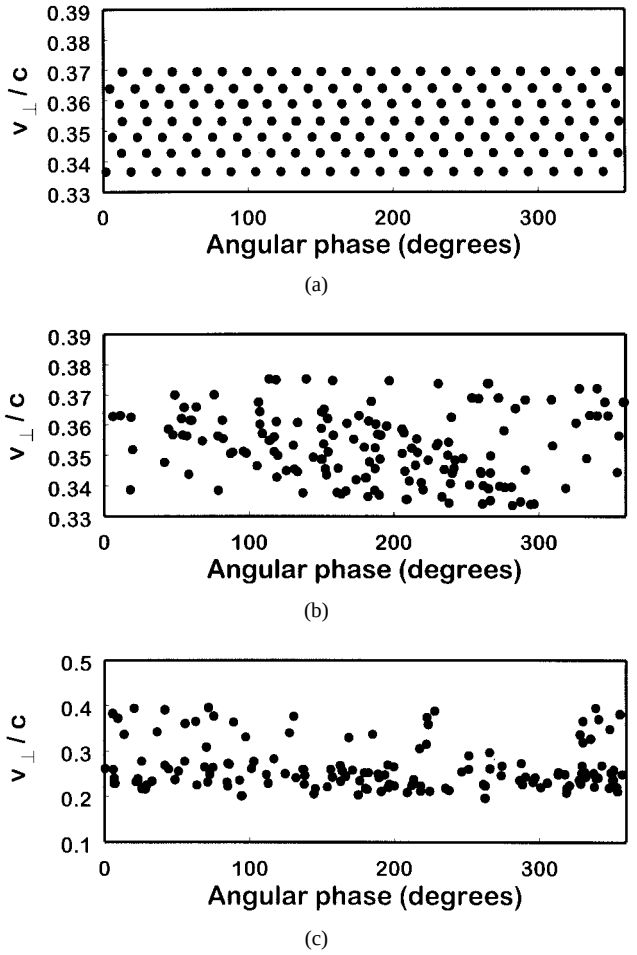

Fig. 3. Representative phase distribution of electrons at (a) output cavity entrance ($P_{in} = 0$ W); (b) output cavity entrance ($P_{in} = 480$ W); and (c) output cavity exit ($P_{in} = 480$ W).

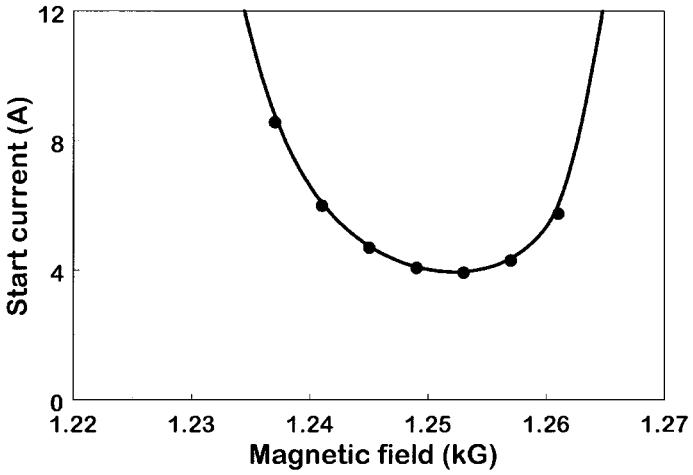

Fig. 4. Output cavity start-oscillation curve for the TE_{021} mode.

velocity represent the effect of finite beam thickness and the velocity spread that results from canonical angular momentum. Fig. 3(b) depicts the distribution at the output cavity entrance when a signal of 480 W is injected into the input cavity. There is a slight increase in perpendicular velocity and the density is clearly enhanced in the half-cycle from 100 to 280°. The phase distribution at the exit of the output cavity that corresponds to the 480 W input case is shown in Fig. 3(c). The phase coherence of the beam is essentially destroyed and a large number of particles have given up a large fraction of their perpendicular energy. A much smaller number of particles have remained at about the same energy level or had their energy increase slightly.

The beam evolution throughout the output cavity is indicated in Fig. 1 where the r-z projection of representative particles are plotted. The figure reveals that while some particles gain energy and increase their Larmor radii, the majority of the particles lose a significant amount of energy. The left wall of the cavity is adjacent to the iron pole piece. The length and radius of the main section are 15 and 3.4 cm, respectively. The nominal operating mode is the TE_{021}. The cavity's diffractive quality factor is about 6320. The resistive quality factor is above 51 000 for a copper cavity, so about 89% of the microwave power can be extracted. Nonlinear tapers are used to change the cavity radius from the main section to the diffractive lip and from the end of the lip to the waveguide radius. These adiabatic transitions are used instead of abrupt transitions to minimize mode conversion to the TE_{01} mode. Both tapers are approximately 1.5 cm long. The length and radius of the diffractive lip are 0.29 and 3.2 cm, respectively.

The start-oscillation curve for the output cavity is given in Fig. 4. The mode with the lowest start current in the frequency range of interest is the desired operating mode. The minimum start current is slightly below 4 A at an axial magnetic field of 1.25 kG. However, this mode is stable at the nominal current of 8 A at the optimal magnetic field value. No other modes appear to present a problem at the nominal design point.

The simulated results for the parameters in Table II near the optimal drive power are summarized in Table III. The nominal electric field at the beam is about 6 kV/cm in the input cavity and over five times that in the output cavity (at the outer edge of the beam where the field is a maximum). The peak electric field at the wall is 13 kV/cm in the input cavity and zero in the output cavity. The total axial velocity spread includes a contribution of about 6.7% from energy spread and about 8.3% from canonical angular momentum. The contribution to the perpendicular velocity spread from the energy spread is small. The nominal saturated gain is about 25.5 dB. The total amplified power is over 185 kW. The peak efficiency of 52% exceeds the performance of any third harmonic small-orbit amplifier to date.

The drive curve for parameters near the optimal configuration is shown in Fig. 5. In accordance with Fig. 4, the tube is zero-drive stable. However, the efficiency rises rapidly to 43% at a drive power of 109 W. The output power varies only weakly for drive powers above 300 W, with the peak power occurring at an input power of 526 W.

The dependence of efficiency on output cavity Q is revealed in Fig. 6(a) for a drive power of 526 W. The output efficiency rises dramatically from ~22 to ~48% as the quality factor is increased from 3600 to 4500. After that point, the efficiency only increases slowly with Q until it reaches its maximum

TABLE III
THIRD HARMONIC SMOG AMPLIFIER PERFORMANCE

Input cavity results	
Input drive power (W)	526
E_z at beam (kV/cm)	5.83
Drift region results	
Bunching Efficiency (%)	46.0
Total Δv_z (%)	10.71
Total $\Delta v_\perp$ (%)	1.61
Energy spread (%)	2.27
Output cavity results	
Power (kW)	187
Efficiency (%)	52.1
Gain (dB)	25.5
E_ϕ at beam (kV/cm)	33.0

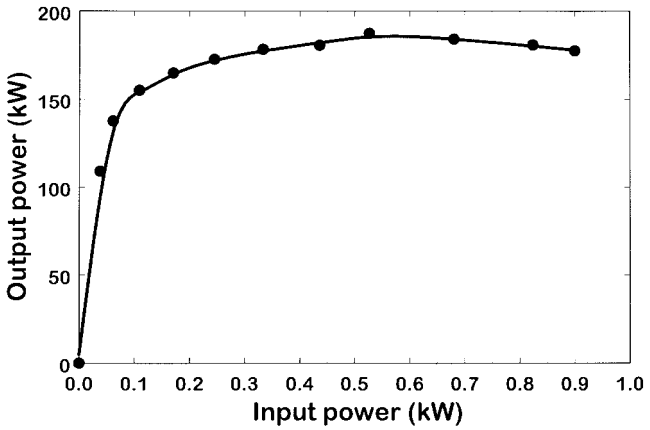

Fig. 5. Dependence of output power on drive power at the optimal system parameters.

value of 52.1% when $Q = 6320$. No amplification is expected for quality factors below 3500.

The dependence of output efficiency on the thin beam's average velocity ratio is given in Fig. 6(b). This ratio is modified solely by varying the magnetic field in the drift region. The phase of the output cavity's electric field is optimized at each point. The amplitude is adjusted to keep the quality factor at the optimal value of 6320. All other parameters, however, are held at their nominal values. The efficiency drops off steadily with decreasing velocity ratio, going to a level of about 33% at a velocity ratio near 1.6. Efficiency decreases slightly above the nominal velocity ratio.

The dependence of the efficiency on the applied magnetic field in the output cavity is given in Fig. 6(c). The efficiency decreases sharply to zero for fields below 1230 G. The decrease in efficiency with increasing field above 1240 G is steady, dropping to 20% at 1275 G. Efficiencies near 50% are maintained only over a range of about 0.6% of the nominal magnetic field. The shape of the magnetic field dependence can be better understood by considering the start-oscillation curve in Fig. 4. Below 1230 G, the required start current rises rapidly due to a decrease in the interaction, and a point is quickly reached where no energy transfer from the beam is possible. The decrease in efficiency is less dramatic on the high side of the optimal field because the start current is still reasonably low.

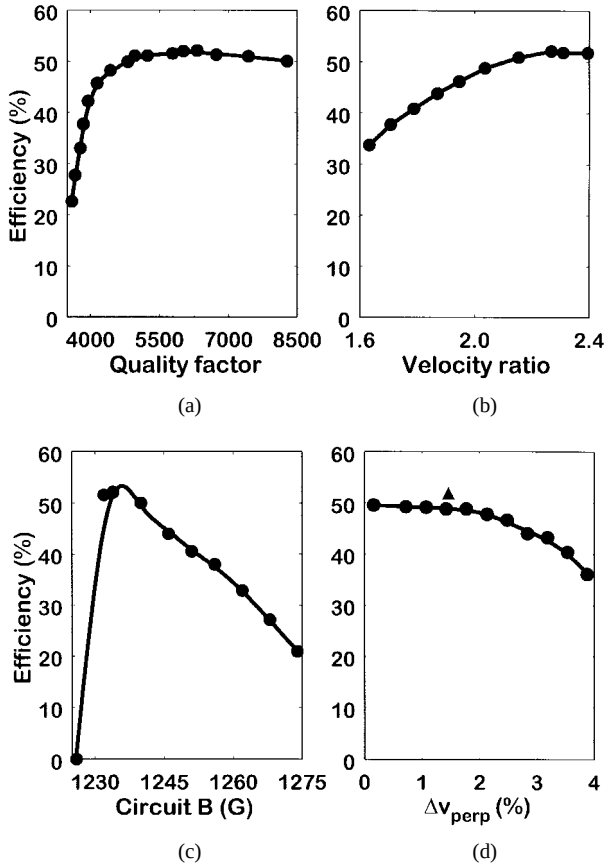

Fig. 6. Dependence of output efficiency on (a) the output cavity quality factor, (b) the average velocity ratio, (c) the magnetic field in the output cavity, and (d) the perpendicular velocity spread.

The dependence of efficiency on perpendicular velocity spread is given in Fig. 6(d). The triangle corresponds to the result produced by the beam from the electron gun. The circles result from an ideal beam where the beam thickness is adjusted to modify the velocity spread. The circuit parameters are held constant at the optimal values. The ideal beam radius is adjusted to match the average velocity ratio from the electron gun's beam. As expected, the efficiency for the realistic beam is close to the result for the ideal beam with a comparable velocity spread. The efficiency decreases slowly up to perpendicular velocity spreads of about 2%, but begins to rapidly fall off after that toward an efficiency of 35% near a spread of 4%. The beam is partially intercepted by the input cavity when the spread exceeds 4%, so it is not possible to calculate efficiencies beyond that point.

IV. SUMMARY

In this work, we have extended previous results to the design of a third-harmonic, prebunched gyrotron experiment. This design has demonstrated that power levels above 185 kW can be generated in X-band with an efficiency in excess of 50% and a gain of approximately 25 dB via the interaction of a 45 kV, 8 A beam, and a novel two-cavity microwave circuit. The peak electric fields in the electron gun and the microwave circuit were easily compatible with CW operation.

The magnetic compression and cathode loading in the annular, Pierce-type gun were also quite conservative.

The numerical modeling was also improved over previous studies in three significant ways. First, the output from the electron gun simulations were input into the "bunching" code to more accurately model the equilibrium distribution of the beam in phase space. Second, the magnetic field profiles from a series of pancake coils were input into the buncher code. This was necessary to accurately model the beam trajectory in the end of the compression region. Finally, the realistic field profiles as calculated by a scattering matrix code were used in both large-signal codes. This modification was perhaps the most important, since the fields in the bunching cavity are quite different than the ideal fields of a closed, right-circular cavity due to the beam aperture.

The third harmonic experiment detailed in this paper is currently under construction. We hope to attempt an experimental confirmation of this concept in the next year. We are also investigating a broadband version of this device which replaces both cavities with traveling wave structures.

REFERENCES

[1] K. E. Kreischer *et al.*, "Experimental study of a high-frequency megawatt gyrotron oscillator," *Phys. Fluids B*, vol. 2, pp. 640–646, 1990.

[2] W. Lawson *et al.*, "Performance characteristics of a high power, X-band, two-cavity gyroklystron," *IEEE Trans. Plasma Sci.*, vol. 20, pp. 216–223, 1992.

[3] G. Gantenbein *et al.*, "Experimental results and numerical simulations of a high power 140 GHz gyrotron," *IEEE Trans. Plasma Sci.*, vol. 22, pp. 861–870, 1994.

[4] K. D. Pendergast, B. G. Danly, R. J. Temkin, and J. S. Wurtele, "Self-consistent simulation of cyclotron autoresonance maser amplifiers," *IEEE Trans. Plasma Sci.*, vol. 16, pp. 122–128, 1988.

[5] V. L. Bratman and G. G. Denisov, "Cyclotron autoresonance masers—Recent experiments and prospects," *Int. J. Electron.*, vol. 72, pp. 969–981, 1992.

[6] G. F. Brand, Y. Idehara, T. Tatsukawa, and I. Ogawa, "Mode competition in a high harmonic gyrotron," *Int. J. Electron.*, vol. 72, pp. 745–758, 1992.

[7] W. Lawson *et al.*, "High power operation of a K-band second harmonic gyroklystron," *Phys. Rev. Lett.*, vol. 71, pp. 456–459, 1993.

[8] D. V. Kisel *et al.*, "An experimental study of a gyrotron operating at the second harmonic of the cyclotron frequency with optimized distribution of the high-frequency field," *Radio Eng. Electron. Phys.*, vol. 19, pp. 95–100, 1974.

[9] P. Sprangle, "Exicitation of electromagnetic waves from a rotating annular relativistic e-beam," *J. Appl. Phys.*, vol. 47, pp. 2935–2940, 1976.

[10] W. W. Destler *et al.*, "Experimental study of microwave generation and suppression in a nonneutral e-layer," *J. Appl. Phys.*, vol. 48, pp. 3291–3296, 1977.

[11] H. S. Uhm and R. C. Davidson, "Intense microwave generation by the negative-mass instability," *J. Appl. Phys.*, vol. 49, pp. 593–598, 1978.

[12] W. W. Destler *et al.*, "Intense microwave generation from a nonneutral rotating E layer," *J. Appl. Phys.*, vol. 52, pp. 2740–2749, 1981.

[13] W. W. Destler, R. L. Weiler, and C. D. Striffler, "High-power microwave generation from a rotating E layer in a magnetron-type waveguide," *Appl. Phys. Lett.*, vol. 38, pp. 570–572, 1981.

[14] W. W. Destler, R. Kulkarni, C. D. Striffler, and R. L. Weiler, "Microwave generation from rotating electron beams in magnetron-type waveguides," *J. Appl. Phys.*, vol. 54, pp. 4152–4162, 1983.

[15] W. Lawson, W. W. Destler, and C. D. Striffler, "High-power microwave generation from a large-orbit gyrotron in vane and hole-and-slot conducting wall geometries," *IEEE Trans. Plasma Sci.*, vol. PS-13, pp. 444–453, 1985.

[16] E. Chojnacki, W. W. Destler, W. Lawson, and W. Namkung, "Studies of microwave radiation from a nonrelativistic rotating electron beam in a multiresonator magnetron cavity," *J. Appl. Phys.*, vol. 61, pp. 1268–1275, 1987.

[17] W. W. Destler *et al.*, "High-power microwave generation from large-orbit devices," *IEEE Trans. Plasma Sci.*, vol. 16, pp. 71–89, 1988.

[18] W. W. Destler *et al.*, "Intense-beam fundamental mode large-orbit gyrotron studies," *J. Appl. Phys.*, vol. 66, pp. 4089–4094, 1989.

[19] C. S. Kou, D. B. McDermott, N. C. Luhmann, Jr., and K. R. Chu, "Prebunched high-harmonic gyrotron," *IEEE Trans. Plasma Sci.*, vol. 18, pp. 343–349, 1990.

[20] K. Irwin, *et al.*, "Second generation, high power, fundamental mode large-orbit gyrotron experiments," *J. Appl. Phys.*, vol. 69, pp. 627–631, 1991.

[21] W. Lawson and W. W. Destler, "The axially modulated, cusp-injected, large-orbit gyrotron amplifier," *IEEE Trans. Plasma Sci.*, vol. 22, pp. 895–901, 1994.

[22] M. J. Rhee and W. W. Destler, "Relativistic electron dynamics in a cusped magnetic field," *Phys. Fluids*, vol. 17, pp. 1574–1581, 1974.

[23] W. Lawson *et al.*, "Design of a high efficiency, low voltage, axially modulated, cusp-injected, second harmonic, X-band gyrotron amplifier," *IEEE Trans. Plasma Sci.*, vol. 24, pp. 678–686, 1996.

[24] W. B. Herrmannsfeldt, "Electron trajectory program," Rep. 226, Stanford Linear Accelerator Center, Stanford, CA, Nov. 1979.

[25] W. Lawson and P. E. Latham, "The scattering matrix formulation for overmoded coaxial cavities," *IEEE Trans. Microwave Theory Tech.*, vol. 40, pp. 1973–1976, 1992.

[26] P. E. Latham, S. M. Miller, and C. D. Striffler, "Generalized form of Madey's theorem for computing the gain in microwave devices," *Phys. Rev. A*, vol. 45, pp. 1197–1206, 1992.

Arnold Liu was born in Columbia, MD, in 1976.

For the past two years he had been working at the Institute for Plasma Research as an undergraduate Research Assistant while pursuing the B.S. degree in electrical engineering at the University of Maryland, College Park. Currently, he is a graduate student at Stanford University, Stanford, CA.

Wes Lawson (S'84–M'85–SM'97) received the B.S. degree in mathematics in 1980, and the B.S., M.S., and Ph.D. degrees in electrical engineering from the University of Maryland, College Park, in 1980, 1981, and 1985, respectively. His dissertation work involved theoretical and experimental studies of microwave generation in various large-orbit gyrotron configurations.

He was with the Electronic Systems Branch of Harry Diamond Laboratories from 1978 to 1982. He has been with the Institute for Plasma Research, University of Maryland, for the past 13 years, and is currently a Professor in the Department of Electrical Engineering. His main interest is in novel fast-wave microwave sources, and his recent efforts have been directed toward high-power fast-wave and hybrid amplifiers and associated high-power microwave components.

Anna Fernandez (S'95) was born in Falls Church, VA, in 1975.

For the past two years, she had been with the Institute for Plasma Research, University of Maryland, College Park, as an undergraduate Research Assistant while pursuing the B.S. degree in electrical engineering. Currently, she is a graduate student at Duke University, Durham, NC.

John Rodgers received the B.S.E.E. degree from the University of Maryland, College Park, in 1987.

He served in the U.S. Navy from 1975 to 1981 as a Communications and Radar Electronics Technician. From 1981 to 1984, he was with the Space Department of the Johns Hopkins Applied Physics Laboratory. Since 1987, he has worked at the University of Maryland as a Faculty Research Assistant in the Laboratory for Plasma Research.

William W. Destler (M'84–SM'90–F'92) received the B.S. degree from the Stevens Institute of Technology, Hoboken, NJ, in 1968 and the Ph.D. degree from Cornell University, Ithaca, NY, in 1972.

He is presently Dean of Engineering at the University of Maryland, College Park. His research interests have been primarily in the areas of high-power microwave sources and advanced accelerator technology, and he is the author or coauthor of over 100 research papers on these and related topics.

Dr. Destler is the recipient of numerous awards for teaching excellence, including the 1989 AT&T/ASEE Award for Excellence in Engineering Education for the Mid-Atlantic States. He is a Fellow of the American Physical Society.